Phys. Status Solidi B **247**, Nos. 11–12, 2953–2957 (2010) / **DOI** 10.1002/pssb.201000339

physica status solidi b
www.pss-b.com
basic solid state physics

Solution-phase exfoliation of graphite for ultrafast photonics

T. Hasan[1], F. Torrisi[1], Z. Sun[1], D. Popa[1], V. Nicolosi[2], G. Privitera[1], F. Bonaccorso[1], and A. C. Ferrari*[,1]

[1] Department of Engineering, University of Cambridge, Cambridge CB3 0FA, UK
[2] Department of Materials, University of Oxford, Oxford OX1 3PH, UK

Received 17 May 2010, revised 25 July 2010, accepted 27 July 2010
Published online 15 September 2010

Keywords graphene, graphene–polymer composite, saturable absorber, ultrafast laser

* Corresponding author: e-mail acf26@cam.ac.uk, Phone: +44 1223 748351, Fax: +44 1223 748351

We exfoliate graphite in both aqueous and non-aqueous environments through mild sonication followed by centrifugation. The dispersions are enriched with monolayers. We mix them with polymers, followed by slow evaporation to produce optical quality composites. Nonlinear optical measurements show ~5% saturable absorption. The composites are then integrated into fiber laser cavities to generate 630 fs pulses at 1.56 μm. This shows the viability of solution phase processing for graphene based photonic devices.

1 Introduction Ultrafast lasers have many applications, ranging from basic research and metrology to telecommunications, medicine, and materials processing. Most employ a mode-locking technique, whereby a nonlinear optical element – called saturable absorber – turns the laser continuous wave into a train of ultrashort pulses. Semiconductor saturable absorber mirrors (SESAMs) currently dominate passive mode-locking [1]. However, these have a narrow tuning range (tens of nanometer), and require complex fabrication and packaging [1]. A simpler and cost-effective alternative relies on single wall carbon nanotubes (SWNTs) [2–7], where the operating wavelength is defined by the SWNT diameter (i.e., bandgap) [2, 4]. Tunability is possible by combining SWNTs with a diameter distribution [5]. However, for a chosen wavelength, the SWNTs not in resonance are not used, and contribute insertion losses, compromising device-performance. Novel nonlinear materials with broadband absorption are therefore required for wideband, tunable operation.

The linear dispersion of Dirac electrons in graphene offers the ideal solution: for any excitation there is an electron–hole pair in resonance. Due to the ultrafast carrier dynamics [8–10] and large absorption of incident light per layer (~2.3% [11, 12]), graphene behaves as a fast saturable absorber over a wide spectral range [2, 13–15]. Unlike SESAMs and SWNTs, graphene saturable absorbers do not need band-gap engineering or chirality/diameter control.

Here, we exfoliate graphite by mild sonication in water with sodium deoxycholate (SDC) bile salt, in anhydrous *N*-methylpyrrolidone (NMP) and in *ortho*-dichlorobenzene (*o*-DCB). Graphene–polymer composites (GPCs) are then prepared and studied by power dependent absorption and integrated into fiber cavities to produce ultrafast laser pulses. These procedures and composites are also useful for a variety of photonic and optoelectronic applications, exploiting the conductivity, transparency, ultra-wide band tunability, and ultrafast dynamics of graphene [13].

2 Experimental Graphite flakes are exfoliated in a sonic bath. To get aqueous dispersions, 1.2 wt% flakes are sonicated for ~3 h with 0.5 wt% SDC. For NMP and *o*-DCB dispersions, 1.2 wt% flakes are sonicated for 6–9 h in sealed glass bottles. The un-exfoliated particles are allowed to settle for 10 min after sonication. The dispersions are then placed in a centrifuge at 10,000 rpm (17,000*g*) for an hour. The top 70% is decanted for characterization and composite fabrication. An aqueous solution with 120 mg polyvinyl alcohol (PVA) is sonicated with 4 ml centrifuged graphite dispersion. Water is then evaporated, leaving a ~50 μm PVA–GPC. For NMP and *o*-DCB dispersions, 200 mg styrene methyl methacrylate (SMMA) solution in NMP(*o*-DCB) is mixed with 2 ml centrifuged NMP(*o*-DCB)-graphite dispersion. NMP(*o*-DCB) is then evaporated in vacuum and then baked in oven at 80 °C, producing ~50 μm SMMA–GPC.

A Perkin-Elmer spectrometer is used for absorption measurements. Raman spectroscopy on dropcast flakes is carried out using a Renishaw spectrometer at 514.5 nm. For transmission electron microscopy (TEM), dispersions are dropped onto a lacey carbon support grid (400 mesh). TEM images are taken using a JEM-3000F FEGTEM at 300 kV. For power-dependent absorption measurements, the GPC is sandwiched between fiber connectors and coupled to a ~600 fs pulsed source centered at 1558 nm. A 20% tap is used to monitor the input power to the connector containing the GPC. Two calibrated power-heads read the input and output simultaneously. A spectrum analyzer and a second harmonic generation (SHG) autocorrelator measure output spectrum and pulse width.

3 Results

3.1 Dispersions Figure 1a is the absorption of the centrifuged dispersions diluted to 10%. The spectra are mostly featureless, as expected [14, 16, 17]. The peak in the UV region is a signature of the exciton-shifted van Hove singularity in the graphene density of states [18]. Absorption spectroscopy may be used to estimate the concentration of SWNTs [19–22] and graphite/graphene flakes [23, 24] from the Beer–Lambert law. Using absorptions of $1390\,\mathrm{L\,g^{-1}\,m^{-1}}$ for graphite-water dispersions and $2460\,\mathrm{L\,g^{-1}\,m^{-1}}$ for NMP and *o*-DCB at 660 nm as empirically determined in Refs. [23, 24], we estimate concentrations of ~0.18, ~0.1, and $\sim 0.06\,\mathrm{g\,L^{-1}}$.

Dispersion and stabilization of nanoparticles such as nanotubes and graphene in pure solvents can be explained by considering the relative solvent–solvent, solvent–particle, and particle–particle interaction strengths [23]. Stable dispersions require the Gibbs free energy of mixing, ΔG_{mix}, to be 0 or negative [25]:

$$\Delta G_{\mathrm{mix}} = \Delta H_{\mathrm{mix}} - T\Delta S_{\mathrm{mix}}, \quad (1)$$

where T is the temperature, ΔH_{mix} is the enthalpy of mixing, and ΔS_{mix} is the entropy change in the mixing process. For large solute particles like graphene and nanotubes, ΔS_{mix} is small [23, 26]. Therefore, for dispersion and stabilization of graphene in solvents, ΔH_{mix} needs to be very small. This can be achieved by choosing a solvent whose surface energy is very close to graphene since for a given graphene volume fraction and flake thickness [23]:

$$\Delta H_{\mathrm{mix}} \propto (\delta_1 - \delta_2)^2, \quad (2)$$

where, δ_i is the square root of surface energy of graphene and solvent. Equation (2) requires the surface energies of graphene and solvent to be very close for a stabilized dispersion. The surface tension (γ) of NMP and *o*-DCB are 35.71 and $44.56\,\mathrm{mJ\,m^{-2}}$ [27]. When converted to solvent surface energy (E_{Sur}) with a generalized surface entropy (S_{Sur}) of $0.1\,\mathrm{mJ\,K^{-1}\,m^{-2}}$ [28, 29] using the relation $\gamma = (E_{\mathrm{Sur}} - TS_{\mathrm{Sur}})$ [29], we get E_{sur} ~65–75 $\mathrm{mJ\,m^{-2}}$. This is within the range of estimated surface energies (~$70\,\mathrm{mJ\,m^{-2}}$) of nanotubes and graphite [23, 26, 30–33] and explains our efficient exfoliation of graphite in NMP and *o*-DCB. The concentrations of flakes in our NMP and *o*-DCB dispersions are ~0.1 and $\sim 0.06\,\mathrm{g\,L^{-1}}$, higher than previous reports [23, 24], as mild sonication for a long period (6–9 h) yields higher loading. NMP, being a

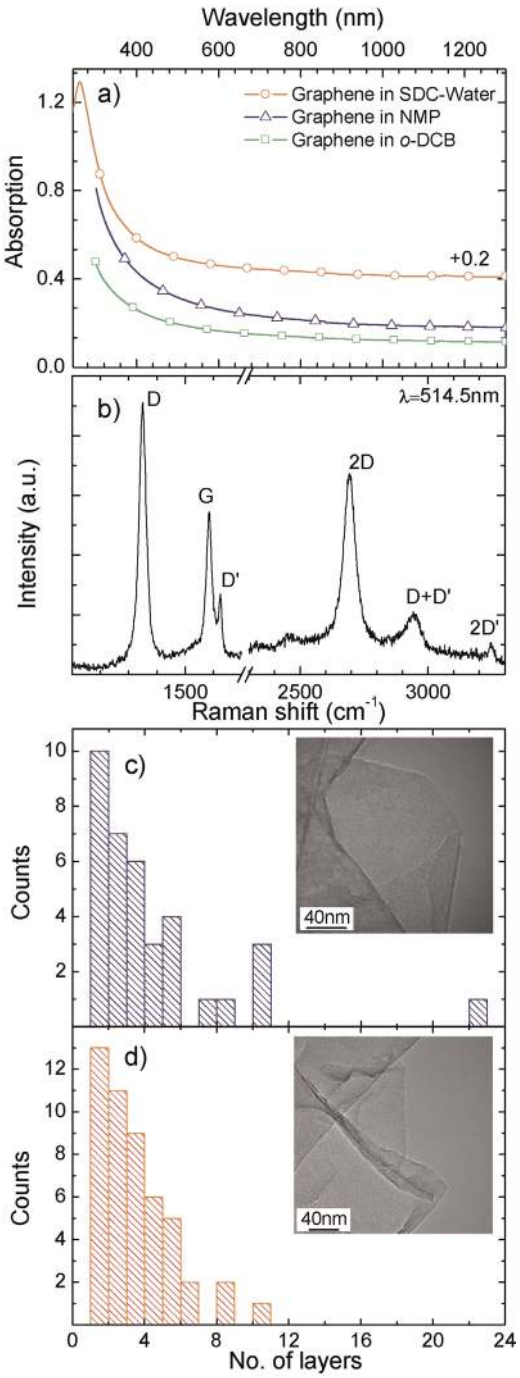

Figure 1 (online color at: www.pss-b.com) (a) Absorption of 10% diluted graphite dispersions in SDC–water, NMP, and *o*-DCB. Solvent and surfactant backgrounds are subtracted. (b) Raman spectrum of a flake on Si. (c) TEM statistics for anhydrous NMP dispersions showing ~50% SLG and BLG. Inset: Folded SLG. (d) TEM statistics for water–SDC dispersions showing ~50% SLG and BLG. Inset: Folded SLG.

hygroscopic solvent, tends to absorb moisture from air [34, 35]. Unless the anhydrous NMP we use is kept tightly sealed, we observe that the concentration of dispersed flakes in NMP drops significantly. E_{Sur} of a binary solvent mixture does not linearly depend on the properties and molar fractions of the pure solvent components [36, 37], but deviates from that of pure solvents depending on the respective molar fractions in the mixture [38]. We thus attribute the reduction in the concentration of dispersed flakes to the absorbed moisture in NMP which changes its E_{Sur}. This underpins the importance of matching δ_1 and δ_2 in Eq. (2) to obtain stable dispersions.

For aqueous dispersions, the surfactant molecular structure plays an important role. We use the SDC bile salt as surfactant because of its rigid cyclopentenophenanthrene nucleus [39]. This has one hydrophobic side with methyl groups (β-side), and one hydrophilic side, the latter containing two hydroyxl groups (α-side) [39]. It also has a short aliphatic chain with a highly hydrophilic termination. Bile salt surfactants, because of their flat molecular structure, adsorb readily on hydrophobic graphite surfaces [39, 40], their β-side having a large contact area (~1.8–3 nm^2) per surfactant molecule [41] compared to linear chain surfactants (e.g., sodium dodecylbenzene sulfonate (SDBS) [24, 42]), which usually adsorbs on graphitic surfaces through its alkyl chains [43]. The bile salts hydrophobicity rules how strongly they are adsorbed on graphitic surfaces, as measured by the hydrophobic index (HI) [44]:

$$\mathrm{HI} = \mathrm{HI}_{\alpha} + \mathrm{HI}_{\beta}, \tag{3}$$

where

$$\mathrm{HI}_{\alpha(\beta)} = \frac{\text{Hydrophobic surface area}_{\alpha(\beta)}}{\text{Hydrophilic surface area}_{\alpha(\beta)}} \times \text{anomer\%}. \tag{4}$$

The HI of deoxycholic acid (7.27) is higher than its trihydroxy counterpart, cholic acid (6.91) [44]. This is also reflected in the higher effective contact area per gram of graphite (defined as the surfactant molecular surface area at the air/water interface × maximum amount of surfactant monolayer absorption × Avogadro constant) with SDC molecules (6.96 $nm^2\,g^{-1}$) compared to sodium cholate (SC) (5.72 $nm^2\,g^{-1}$) [41], implying a denser and more regular coverage with SDC. Di-hydroxy salts, e.g., SDC or sodium taurodeoxycholate (TDC) are thus expected to be more effective than trihydroxy ones, e.g., SC or sodium taurocholate (TC), and significantly better than linear chain surfactants such as SDBS due to their linear alkyl chain. Thermodynamic parameters of bile salts adsorbing on graphite at 25–30 °C show that ΔG_{mix} for SDC adsorbed on graphite (~28 kJ mol^{-1} [40]) is more negative than for SC ($\Delta G_{mix} \sim -26$ kJ mol^{-1} [40]). Equation (1) dictates the thermodynamic stability of solutions or dispersions. It indicates that graphene flakes dispersed by SDC in water will be more stable compared to SC–water [40].

The Raman spectrum of a representative flake from a water–SDC dispersion is given in Fig. 1b. Besides the G and 2D peaks, this has significant D and D′ intensities. The G peak corresponds to the E_{2g} phonon at the Brillouin zone center. The D peak is due to the breathing modes of sp^2 rings and requires a defect for its activation by double resonance (DR) [45–47]. The 2D peak is the second order of the D peak. This is a single band in single layer graphene (SLG), whereas it splits in four in bi-layer graphene (BLG), reflecting the evolution of the band structure [45]. The 2D peak is always seen, even when no D peak is present, since no defects are required for the activation of two phonons with the same momentum, one backscattering from the other. DR can also happen intra-valley, i.e., connecting two points belonging to the same cone around **K** or **K′**, giving the D′ peak. The large D intensity in Fig. 1b is not due to a large amount of disorder, otherwise it would be much broader, and G, D′ would merge [46]. We rather assign it to edges of our sub-micrometer flakes [48]. We note that 2D, although broader than in pristine graphene [45], is still a single Lorentzian. Thus, even Fig. 1b is a multi-layer, it electronically behaves as decoupled SLGs [49], consistent with the folded SLG seen in TEM (Fig. 1c and d).

TEM shows the presence of ~300–600 nm wide SLGs, BLGs, and few layer graphene (FLG) flakes. TEM statistics gives ~28% SLG, ~19% BLGs in NMP (Fig. 1c); ~26 and ~22% in water–SDC (Fig. 1d). Amongst BLGs, ~60% are AB-stacked, while ~40% are folded SLGs (Fig. 1c and d).

3.2 Composites Optical microscopy reveals no large aggregates in the PVA–GPCs (Fig. 2b). This is important to avoid scattering losses [50], in view of their use as saturable absorbers [2, 13–15]. Normalized nonlinear absorption measurements at 1558 nm are shown in Fig. 2b. At low input power, the absorption is almost independent on pump power. However, it decreases ~5% when the power raises to 5.35 mW (i.e., for a peak power density of ~266 MW cm^{-2}). This is an indication of saturable absorption [2, 14, 15].

3.3 Ultrafast pulse generation We then use the composite to prepare a mode-locker, Fig. 2a, by sandwiching a PVA–GPC between two fiber connectors. A 0.8 m erbium doped fiber (EDF) is used as gain medium, pumped by a 980 nm diode laser via a wavelength division multiplexer. An isolator is placed after the gain fiber to ensure unidirectional operation. A polarization controller optimizes mode-locking. The full width at half maximum (FWHM) of a typical output spectrum is 4 nm (Fig. 2c). The sidebands are due to intracavity periodical perturbations, typical of soliton-like pulse formation [51]. The SHG autocorrelation trace (Fig. 2d) of the output pulses has FWHM ~970 fs. Considering a $sech^2$ temporal profile, a 630 fs pulse width is obtained [52]. The time bandwidth product (TBP) is a measure of the output pulse quality and is a product of pulse duration (in seconds) and spectral width (in Hertz). The TBP is ~0.31, close to the theoretical value of 0.315 for Fourier transform limited $sech^2$ pulses [52].

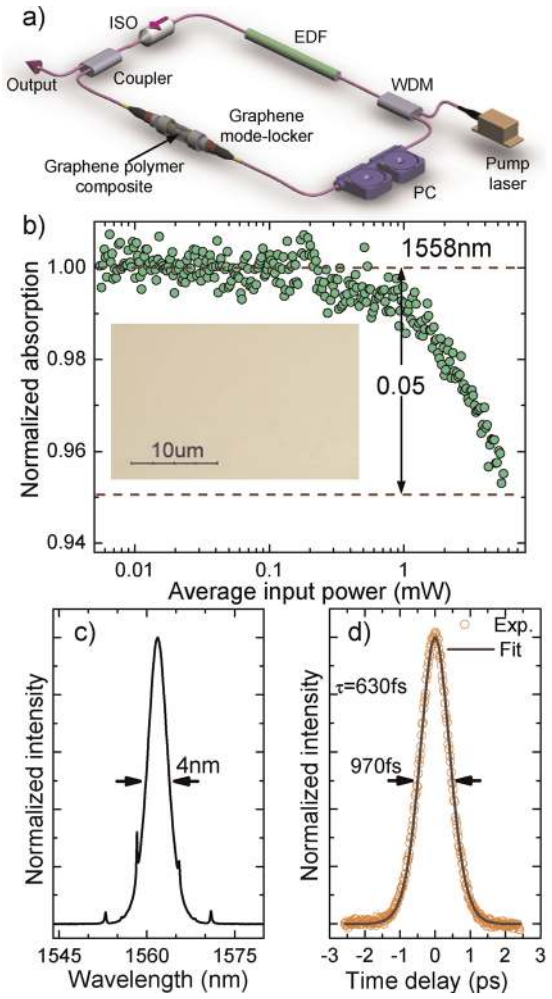

Figure 2 (online color at: www.pss-b.com) (a) Fiber laser setup. WDM, wavelength division multiplexer; EDF, erbium doped fiber; ISO, isolator; PC, polarization controller. The GPC is sandwiched between the connectors. (b) Nonlinear absorption at 1558 nm. Inset: Optical micrograph of a PVA-GPC. (c) Output spectrum of the mode-locked pulse centered at 1562 nm, with 4 nm spectral width. (d) Autocorrelation trace with $sech^2$ fit. The pulse width is 630 fs.

The repetition rate is 19.9 MHz, as determined by the cavity length.

4 Conclusion We achieved efficient liquid-phase exfoliation of graphite. This strongly depends on the solvent surface energies in non-aqueous media, and surfactant molecular structure in water. The polymer composites prepared from these dispersions show nonlinear saturable absorption, allowing us to mode-lock a laser with 630 fs pulses. Liquid phase exfoliation of graphite is an economic, easily scalable alternative to direct growth of graphene, or micromechanical exfoliation, and must be considered not only for photonic devices, but more generally when cost reduction is crucial.

Acknowledgements We acknowledge funding from EPSRC EP/G030480/1, EP/G042357/1 the ERC grant NANOPOTS, a Brian Mercer Award for Innovation. TH acknowledges funding from King's College, FB from a Newton International Fellowship, VN from the Royal Academy of Engineering/EPSRC, ACF is a Royal Society Wolfson Research Merit Award holder.

References

[1] U. Keller, Nature **424**, 831 (2003).
[2] T. Hasan, Z. Sun, F. Wang, F. Bonaccorso, P. H. Tan, A. G. Rozhin, and A. C. Ferrari, Adv. Mater. **21**, 3874 (2009).
[3] Z. Sun, A. G. Rozhin, F. Wang, T. Hasan, D. Popa, W. O'Neill, and A. C. Ferrari, Appl. Phys. Lett. **95**, 253102 (2009).
[4] V. Scardaci, Z. Sun, F. Wang, A. G. Rozhin, T. Hasan, F. Hennrich, I. H. White, W. I. Milne, and A. C. Ferrari, Adv. Mater. **20**, 4040 (2008).
[5] F. Wang, A. G. Rozhin, V. Scardaci, Z. Sun, F. Hennrich, I. H. White, W. I. Milne, and A. C. Ferrari, Nat. Nanotechnol. **3**, 738 (2008).
[6] Z. Sun, A. G. Rozhin, F. Wang, V. Scardaci, W. I. Milne, I. H. White, F. Hennrich, and A. C. Ferrari, Appl. Phys. Lett. **93**, 061114 (2008).
[7] Z. Sun, T. Hasan, F. Wang, A. Rozhin, I. White, and A. Ferrari, Nano Res. **3**, 404 (2010).
[8] M. Breusing, C. Ropers, and T. Elsaesser, Phys. Rev. Lett. **102**, 086809 (2009).
[9] D. Sun, Z.-K. Wu, C. Divin, X. Li, C. Berger, W. A. de Heer, P. N. First, and T. B. Norris, Phys. Rev. Lett. **101**, 157402 (2008).
[10] K. Seibert, G. C. Cho, W. Kütt, H. Kurz, D. H. Reitze, J. I. Dadap, H. Ahn, M. C. Downer, and A. M. Malvezzi, Phys. Rev. B **42**, 2842 (1990).
[11] R. R. Nair, P. Blake, A. N. Grigorenko, K. S. Novoselov, T. J. Booth, T. Stauber, N. M. R. Peres, and A. K. Geim, Science **320**, 1308 (2008).
[12] C. Casiraghi, A. Hartschuh, E. Lidorikis, H. Qian, H. Harutyunyan, T. Gokus, K. S. Novoselov, and A. C. Ferrari, Nano Lett. **7**, 2711 (2007).
[13] F. Bonaccorso, Z. Sun, T. Hasan, and A. C. Ferrari, Nat. Photonics **4**, 611 (2010).
[14] Z. Sun, T. Hasan, F. Torrisi, D. Popa, G. Privitera, F. Wang, F. Bonaccorso, D. M. Basko, and A. C. Ferrari, ACS Nano **4**, 803 (2010).
[15] Z. Sun, D. Popa, T. Hasan, F. Torrisi, F. Wang, E. J. R. Kelleher, J. C. Travers, V. Nicolosi, and A. C. Ferrari, Nano Res. **3**, 653 (2010).
[16] K. F. Mak, M. Y. Sfeir, Y. Wu, C. H. Lui, J. A. Misewich, and T. F. Heinz, Phys. Rev. Lett. **101**, 196405 (2008).
[17] T. Eberlein, U. Bangert, R. R. Nair, R. Jones, M. Gass, A. L. Bleloch, K. S. Novoselov, A. Geim, and P. R. Briddon, Phys. Rev. B **77**, 233406 (2008).
[18] V. G. Kravets, A. N. Grigorenko, R. R. Nair, P. Blake, S. Anissimova, K. S. Novoselov, and A. K. Geim, Phys. Rev. B **81**, 155413 (2010).
[19] T. Hasan, V. Scardaci, P. H. Tan, A. G. Rozhin, W. I. Milne, and A. C. Ferrari, J. Phys. Chem. C **111**, 12594 (2007).
[20] T. Hasan, P. H. Tan, F. Bonaccorso, A. Rozhin, V. Scardaci, W. Milne, and A. C. Ferrari, J. Phys. Chem. C **112**, 20227 (2008).
[21] S. Giordani, S. D. Bergin, V. Nicolosi, S. Lebedkin, M. M. Kappes, W. J. Blau, and J. N. Coleman, J. Phys. Chem. B **110**, 15708 (2006).

[22] B. J. Landi, H. J. Ruf, J. J. Worman, and R. P. Raffaelle, J. Phys. Chem. B **108**, 17089 (2004).
[23] Y. Hernandez, V. Nicolosi, M. Lotya, F. M. Blighe, Z. Sun, S. De, I. T. McGovern, B. Holland, M. Byrne, Y. K. Gun'Ko, J. J. Boland, P. Niraj, G. Duesberg, S. Krishnamurthy, R. Goodhue, J. Hutchison, V. Scardaci, A. C. Ferrari, and J. N. Coleman, Nat. Nanotechnol. **3**, 563 (2008).
[24] M. Lotya, Y. Hernandez, P. J. King, R. J. Smith, V. Nicolosi, L. S. Karlsson, F. M. Blighe, S. De, Z. Wang, I. T. McGovern, G. S. Duesberg, and J. N. Coleman, J. Am. Chem. Soc. **131**, 3611 (2009).
[25] C. M. Hansen, Hansen Solubility Parameters: A User's Handbook (CRC Press Inc., Boca Raton, FL, 2007).
[26] S. D. Bergin, V. Nicolosi, P. V. Streich, S. Giordani, Z. Sun, A. H. Windle, P. Ryan, N. P. P. Niraj, Z.-T. Wang, L. Carpenter, W. J. Blau, J. J. Boland, J. P. Hamilton, and J. N. Coleman, Adv. Mater. **20**, 1876 (2008).
[27] C. L. Yaws, Thermophysical Properties of Chemicals and Hydrocarbons (William Andrew Inc., Norwich, NY, 2008).
[28] M. H. Ghatee and L. Pakdel, Fluid Phase Equil. **234**, 101 (2005).
[29] J. Lyklema, Colloids Surf. A **156**, 413 (1999).
[30] R. Zacharia, H. Ulbricht, and T. Hertel, Phys. Rev. B **69**, 155406 (2004).
[31] L. A. Girifalco and R. A. Lad, J. Chem. Phys. **25**, 693 (1956).
[32] S. B. Trickey, F. Müller-Plathe, G. H. F. Diercksen, and J. C. Boettger, Phy. Rev. B **45**, 4460 (1992).
[33] M. C. Schabel and J. L. Martins, Phys. Rev. B **46**, 7185 (1992).
[34] C. M. White, P. C. Rohar, G. A. Veloski, and R. R. Anderson, Energy & Fuels **11**, 1105 (1997).
[35] P. Kneisl and J. W. Zondlo, J. Chem. Eng. Data **32**, 11 (1987).
[36] J. Escobedo and G. A. Mansoori, AlChE J. **44**, 2324 (1998).
[37] P. Rice and A. S. Teja, J. Colloid Interface Sci. **86**, 158 (1982).
[38] M. a, J. Dávila, R. Alcalde, and S. Aparicio, Ind. Eng. Chem. Res. **48**, 1036 (2008).
[39] D. M. Small, S. A. Penkett, and D. Chapman, Biochim. Biophys. Acta **176**, 178 (1969).
[40] G. Sugihara, D.-S. Shigematsu, S. Nagadome, S. Lee, Y. Sasaki, and H. Igimi, Langmuir **16**, 1825 (2000).
[41] Y. Sasaki, T. Igura, Y. I. Miyassu, S. Lee, S. Nagadome, H. Takiguchi, and G. Sugihara, Colloids Surf. B **5**, 241 (1995).
[42] S. De, P. J. King, M. Lotya, A. O'Neill, E. M. Doherty, Y. Hernandez, G. S. Duesberg, and J. N. Coleman, Small **6**, 458 (2010).
[43] M. F. Islam, E. Rojas, D. M. Bergey, A. T. Johnson, and A. G. Yodh, Nano Lett. **3**, 269 (2003).
[44] K. Miyajima, J. Chem. Soc. **84**, 2537 (1988).
[45] A. C. Ferrari, J. C. Meyer, V. Scardaci, C. Casiraghi, M. Lazzeri, F. Mauri, S. Piscanec, D. Jiang, K. S. Novoselov, S. Roth, and A. K. Geim, Phys. Rev. Lett. **97**, 187401 (2006).
[46] A. C. Ferrari and J. Robertson, Phys. Rev. B **61**, 14095 (2000).
[47] F. Tuinstra and J. L. Koenig, J. Chem. Phys. **53**, 1126 (1970).
[48] C. Casiraghi, A. Hartschuh, H. Qian, S. Piscanec, C. Georgi, A. Fasoli, K. S. Novoselov, D. M. Basko, and A. C. Ferrari, Nano Lett. **9**, 1433 (2009).
[49] S. Latil, V. Meunier, and L. Henrard, Phys. Rev. B **76**, 201402 (2007).
[50] C. F. Bohren and D. R. Huffman, Absorption and Scattering of Light by Small Particles (Wiley, New York, 1998).
[51] M. L. Dennis and I. N. Duling, IEEE J. Quantum Electron. **30**, 1469 (1994).
[52] G. P. Agrawal, Nonlinear Fiber Optics (Academic Press, New York, 2001).